Dispersion multiplexing with broadband filtering for miniature spectrometers

E. C. Cull, M. E. Gehm, D. J. Brady, C. R. Hsieh, O. Momtahan, and A. Adibi

We replace the traditional grating used in a dispersive spectrometer with a multiplex holographic grating to increase the spectral range sensed by the instrument. The multiplexed grating allows us to measure three different, overlapping spectral bands on a color digital focal plane. The detector's broadband color filters, along with a computational inversion algorithm, let us disambiguate measurements made from the three bands. The overlapping spectral bands allow us to measure a greater spectral bandwidth than a traditional spectrometer with the same sized detector. Additionally, our spectrometer uses a static coded aperture mask in the place of a slit. The aperture mask allows increased light throughput, offsetting the photon loss at the broadband filters. We present our proof-of-concept dispersion multiplexing spectrometer design with experimental measurements to verify its operation.

OCIS codes: 120.620, 090.1970.

1. Introduction

Current environmental sensing, defense, and research applications demand compact and inexpensive spectrometers that maintain a high level of performance. We have designed a spectrometer to meet this goal by using aperture coding and dispersion multiplexing with broadband filtering.

A traditional dispersive spectrometer is composed of three primary elements: an input aperture, a digital focal plane, and a dispersive element. Other optics are usually present, optimized to relay light between the primary elements while minimizing optical aberrations. This spectrometer is operated under the assumption that uniform, spatially incoherent light fully fills the aperture. To achieve reasonable spectral resolution, this requires the aperture to be a spatial filter (typically a slit) to limit the angular extent of the source input to the spectrometer. When examining a diffuse source, the slit blocks the majority of the photons incident on the instrument, limiting light throughput to the spectrometer. This is one of the major trade-offs in slit-based dispersion spectrometer design: spectral resolution versus light throughput. Increasing light throughput in a slit spectrometer while maintaining spectral resolution requires a taller slit and detector, effectively increasing the size and cost of the system. One solution to this problem is to replace the slit with a coded mask with many times the open area of a single slit.

The most expensive single part of a dispersion spectrometer is typically the detector array. The primary reason for this is the demand for spectrometers with the sensitivity to measure low-intensity samples. This challenge is exacerbated by the resolution-throughput trade-off in a slit-based device. A secondary reason for the high cost of spectroscopy detector arrays is their nonstandard aspect ratio. Detector arrays produced in high volume typically use an aspect ratio of 4:3 or 16:9, to be used in consumer imaging devices. Many spectrometers use a noncommodity detector with an aspect ratio of 4:1 or more to increase the number of detector elements along the dispersion axis, thereby increasing spectral resolution. Dispersion multiplexing allows us to use a standard aspect-ratio focal plane by overlaying several spectral ranges across the dispersion axis of the detector. One commercial system uses a form of dispersion multiplexing by dispersing two spectral ranges along discrete stripes, separated along the nondispersion axis of the CCD.[1] (They do, however,

E. C. Cull, M. E. Gehm, and D. J. Brady (dbrady@duke.edu) are with the Duke University Fitzpatrick Institute for Photonics, Box 90291, Durham, North Carolina 27708. C. R. Hsieh, O. Momtahan, and A. Adibi (adibi@ece.gatech.edu) are with the Georgia Institute of Technology, Atlanta, Georgia 30332-0250.

Received 27 March 2006; revised 8 September 2006; accepted 25 September 2006; posted 28 September 2006 (Doc. ID 69352); published 4 January 2007.

0003-6935/07/030365-10$15.00/0

use a standard spectroscopy detector array.) Our technique uses a transmissive holographic grating with multiple grating periods recorded in it to simultaneously disperse three spectral ranges across the entire extent of the detector.

This paper describes a doubly multiplexed spectrometer, using both aperture coding and dispersion multiplexing. This system does not directly measure the spectrum such as a traditional dispersive spectrometer. Our multiplex spectrometer is a computational sensor that measures a combination of components of the input spectrum at each pixel location, which can be processed to provide a spectral measurement. In this paper, we discuss the design and implementation of this dispersion multiplexing spectrometer. The next section describes the theory and inversion procedure used with our Hadamard-coded aperture. Section 3 contains the central point of this manuscript, a description of dispersion multiplexing with broadband filtering for spectrometer miniaturization, followed by a section on our specific system design. We discuss the experimental performance of our device in the fifth section and conclude in the sixth.

2. Coded Aperture Spectroscopy

Replacing the slit used in the aperture of a traditional dispersion-based spectrometer with a two-dimensional coded aperture with many openings allows us to overcome the trade-off between spectral resolution and light throughput faced by spectrometer designers. This is particularly advantageous for systems used to measure the spectra of diffuse sources, since the constant radiance theorem states that light from a diffuse, incoherent source cannot be focused or have its intensity increased through (de)magnification.[2] Other techniques used in spectroscopic instruments to overcome the resolution-throughput trade-off include the use of a structured fiber bundle for light collection or interferometric-based (nondispersive) techniques.[3,4] Neither of these techniques are useful for a low cost spectrometer. The fiber bundle can collect light over a large aperture on one end, but on the other, the bundle must be stacked to imitate the shape of a slit, requiring large optics and a detector for a large collection area. The design stability and tolerances for interferometric spectrometers make them prohibitively expensive when compared to a dispersion-based device.

Coded aperture spectrometers, introduced as multislit spectrometers, were initially implemented with single-channel detectors and moving masks.[5–7] These devices were used to increase light throughput without loss of spectral resolution. Eventually, an entire class of spectrometer was developed known as the Hadamard transform spectrometer (HTS).[8] The basis for the HTS was a moving mask (or set of masks) with a series of openings based on the Hadamard matrix. The primary disadvantage of the HTS systems using a single-channel detector is the time required to take the measurement—each spectral measurement requires a full set of detector measurements for each position of the moveable mask. Since multichannel detectors have become widely available, coded aperture spectrometers have been implemented with spatial light modulators (SLM) and microelectromechanical mirror (MEM) arrays to simulate the moving masks.[9,10] With a two-dimensional aperture code and a two-dimensional array detector, it is possible to measure the spectrum with single shot. Our design uses a static coded aperture made of a two-dimensional chrome pattern deposited on glass, a simpler and more cost effective solution than the MEM- and SLM-based designs. Below, we discuss the theory behind our coding scheme. A more detailed discussion can be found in a prior publication.[11]

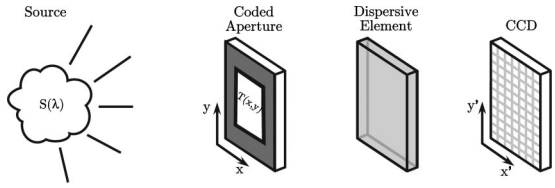

Fig. 1. System diagram showing coordinate systems.

Figure 1 shows a simple schematic of a coded aperture spectrometer and defines the coordinate systems used in this section. Light incident on the detector plane can be represented by

$$I(x',\ y') = \int\int\int \delta(x - (x' + \alpha(\lambda - \lambda_c)))\delta(y - y') \times T(x,\ y)S(x,\ y;\ \lambda)\mathrm{d}x\mathrm{d}y\mathrm{d}\lambda. \quad (1)$$

Here, $\delta(x - (x' + \alpha(\lambda - \lambda_c)))$ is the propagation kernel for a dispersive spectrometer with no internal magnification and with linear dispersion of α along the x axis and center wavelength of λ_c at $x = 0$ for all y. $T(x, y)$ represents the transmittance function of a two-dimensional aperture mask, and $S(x, y; \lambda)$ represents the spectral density as a function of position in the aperture. Since this paper focuses on a spectrometer and not a hyperspectral imager, we assume that there is no spatial structure in the input spectrum of the aperture. This means that $S(x, y; \lambda)$ is constant in x and y, reducing the spectral density to $S(\lambda)$. This reduces Eq. (1) to

$$I(x',\ y') = \int T(x,\ y')S\left(\lambda = \frac{x - x'}{\alpha} + \lambda_c\right)\mathrm{d}x. \quad (2)$$

This means that the intensity measured at the detector is a one-dimensional convolution between the spectrum of the source and the transmittance function of the aperture measured along the dispersion axis of the detector. For a slit-based dispersive spectrometer with the slit at $x = x_0$, $T(x, y)$ can be approximated by a delta function, $\delta(x - x_0)$, so that one position in x' on the detector corresponds to the intensity at a single wavelength:

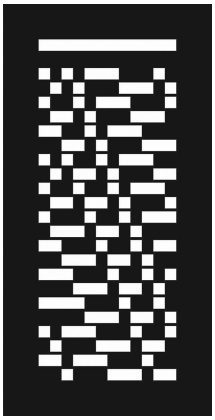

Fig. 2. Diagram of a row-doubled Hadamard aperture mask based on an order-12 Hadamard matrix. White areas indicate light transmission, and black areas indicate where light is blocked.

$$I(x',\ y') = S\left(\lambda = \frac{x_0 - x'}{\alpha} + \lambda_c\right). \tag{3}$$

Using a coded transmittance pattern for $T(x, y)$ causes the instrument to become a multiplex device such that one position on the detector in (x', y') measures the sum of the intensities at several wavelengths. This $T(x, y)$ must be properly designed to yield an accurate estimation of the source spectrum.

Previously, we have shown that mask transmittance patterns based on families of orthogonal functions are sufficient for the design requirements of a system based on a coded aperture mask.[11] Traditionally, the Hadamard matrix has been used as the basis for coded aperture spectrometers. The order-p Hadamard matrix is an orthogonal matrix with p rows, originally derived as an optimal solution for making a multiplex measure of several weights in the presence of noise.[8,12] A mask based on an order-12 Hadamard matrix is shown in Fig. 2. While the order-12 Hadamard matrix has 12 rows, this mask has been constructed according to a previously published row-doubling procedure, yielding the 24 rows shown in the figure.[11]

In a dispersive spectrometer, a coded aperture system decouples spectral resolution from light throughput. For a traditional slit-based spectrometer, a required minimum spectral resolution specifies a maximum slit width, w. A system based on a coded aperture achieves the same spectral resolution by using a feature size of w, where feature size refers to the size of one of the open elements in the aperture mask. Since the coded aperture is constructed of a number of these open elements, it has a larger entrance aperture area and therefore higher light throughput versus the slit. For an aperture based on the order-p Hadamard matrix, there is a 50% loss of light because half of the mask features are opaque. This means that the Hadamard-code-based system achieves $p/2$ times the light throughput of the traditional system when considering a diffuse source that fully fills the input aperture. Further, a finer-pitched mask pattern covering the same aperture area as the original pattern maintains the same light throughput but increases the spectral resolution of the coded aperture spectrometer.

To recover the target spectrum, we take the data from the detector, subtract a dark image to reduce the pattern noise, and then slightly shift each row to correct for the "smile" distortion present in grating spectrometers.[13] The smile distortion can be easily characterized by looking at a target with distinct spectral features such as a gas discharge lamp. It is also possible to reduce smile distortion by introducing a "negative" curvature to the aperture pattern when fabricating the mask, a technique currently used in some slit spectrometers. Generally, we design our aperture mask such that a single mask element covers several pixels on the detector. The last step before inversion is to average the set of pixel rows (along the nondispersion axis of the spectrometer) that make up a single mask feature. The result for a mask with r rows is a set of r data vectors with length corresponding to the number of pixels along the dispersion axis of the detector. A mathematical formulation of this is shown in the following equation, where the rows of M are the data vectors from the detector, the rows of W are spectral estimates formed for each row of input data, and H is the matrix representation of the aperture code.

$$\mathbf{H} \cdot \mathbf{W} = \mathbf{M}. \tag{4}$$

A nonnegative least-squares inversion algorithm is used to calculate the spectra in W. (Typically, we use the LSQNONNEG function built into MATLAB.) We then average these r spectral estimates to determine the spectrum of the target. A more detailed discussion of the coded aperture spectral reconstruction algorithm can be found in a prior publication by our group.[14]

3. Dispersion Multiplexing

In a traditional slit-based dispersion spectrometer, the source spectrum is spread across the detector. A one-dimensional detector is sufficient to record the entire spectrum, though a two-dimensional detector is frequently used to increase the signal-to-noise ratio. For a fixed size detector and a target spectral range, this traditional spectrometer system design is completely specified—the maximum spectral resolution is set by the number of pixels on the detector along the dispersion axis. (Aberrations in the relay optics and a slit width not optimized for maximum spectral resolution can, however, reduce the spectral resolution.) To increase spectral resolution, one must either decrease the spectral range of interest or replace the detector with a higher resolution (and more expensive) model. Assuming the use of a two-dimensional detector, dispersion multiplexing provides an alternative that can increase spectral resolution with the same detector and the same spectral range.

Holographic gratings are useful for dispersion multiplexing spectrometers due to their flexibility in implementing different dispersion patterns. One

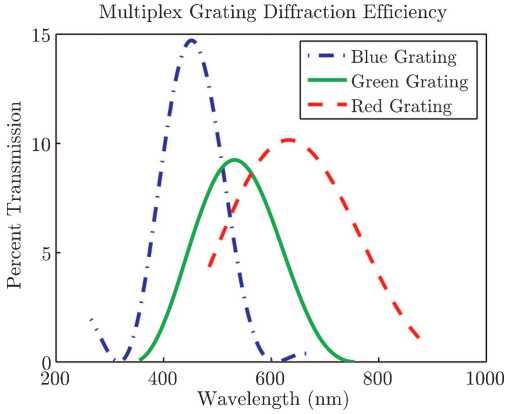

Fig. 3. (Color online) Spectral responses of each grating recorded in the hologram due to Bragg selectivity.

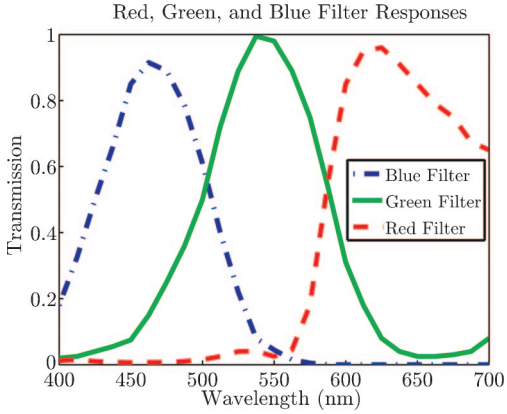

Fig. 5. (Color online) Spectral response of Bayer filters.

commercial system, the Kaiser Holoplex, disperses two separate spectral bands on the detector, each covering a different spectral range.[15] The spectral bands are separated along the nondispersion axis of the detector. Our system uses a multiplex holographic grating with three different grating periods. The Bragg wavelength selectivity of the hologram is tuned so that each of the gratings responds to a different spectral band, as shown in Fig. 3. The grating periods are set to disperse the spectral range of each band fully across the detector.

This results in three spectral bands incident on the same detector pixels. To disambiguate these overlapping bands, we use broadband filters that match the spectral range for each band. While it is possible to implement this type of dispersion multiplexing spectrometer with a set of disambiguation filters external to the detector, we chose to use a simpler and more cost effective color CCD. This combines the broadband filters and detector into a single component. A typical color digital focal plane records data in three spectral bands by using an array of red, green, and blue (RGB) per-pixel filters. The standard pattern of RGB filters used on a color focal plane is known as the Bayer pattern, as shown in Fig. 4.[16] This filter pattern provides one sample of green in each column of the detector and one sample of red and blue in alternating columns of the detector. For a detector with N pixels along the dispersion axis of the detector, this yields N samples of the green spectral band and $N/2$ samples for each of the red and blue spectral bands for our system.

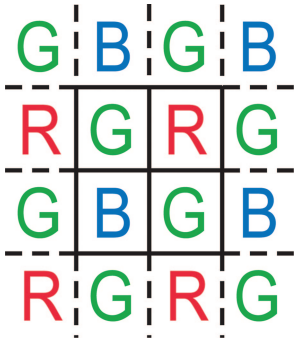

Fig. 4. (Color online) Bayer filter pattern. Each square represents a pixel, and each letter represents either a red, green, or blue filter.

The spectral responses of the Bayer pattern filters used in our system are shown in Fig. 5. These responses are typical of filters used in RGB color imaging. The red-filtered pixels provide an estimate of the spectrum within the red spectral band. Similarly, the green- and blue-filtered pixels estimate their respective spectral bands. As shown in Fig. 5, the RGB filter responses overlap. This causes the three spectral ranges sensed by our dispersion multiplexing spectrometer to overlap. It is necessary to correct for this overlap to eliminate spurious spectral features from our final spectral estimate.

If we assume, in a traditional dispersion spectrometer, that the dispersion direction of the instrument corresponds to the horizontal axis of the detector, then each column of the detector represents a specific element of spectral resolution. A single column of the detector in our dispersion multiplexing spectrometer corresponds to three elements of spectral resolution—one for each of the spectral bands on the detector. Since the per-pixel filter functions are smooth, we can label a column's spectral resolution elements for a column its center wavelength: λ_r, λ_g, and λ_b. In our system we treat every two columns on the detector as one column of output data, giving us one sample of red and blue and two of green for each element of spectral resolution. If we record the values (R, G, B) for one effective column of the detector then we can calculate the proper values, accounting for overlap in the spectral bands, (r, g, b) by solving Eq. (5). The $F_{\text{color}}(\lambda)$ represents the value of the R, G, or B filter functions at the wavelength corresponding to the particular column of the detector.

$$
\begin{aligned}
R &= rF_{\text{red}}(\lambda_r) + gF_{\text{red}}(\lambda_g) + bF_{\text{red}}(\lambda_b),\\
G &= rF_{\text{green}}(\lambda_r) + gF_{\text{green}}(\lambda_g) + bF_{\text{green}}(\lambda_b),\\
B &= rF_{\text{blue}}(\lambda_r) + gF_{\text{blue}}(\lambda_g) + bF_{\text{blue}}(\lambda_b). \qquad (5)
\end{aligned}
$$

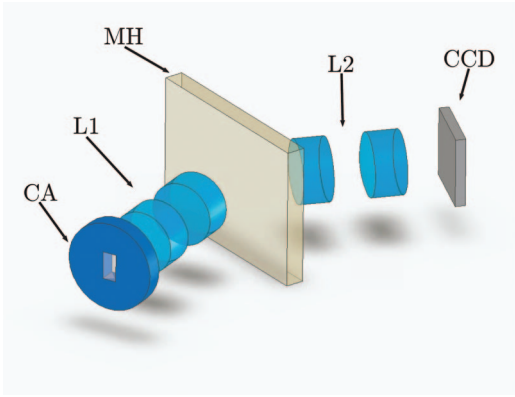

Fig. 6. (Color online) Optical component layout of the dispersion multiplexing spectrometer.

We use a nonnegative least-squares solving algorithm to recover (r, g, b) from (R, G, B).

4. System Design

The layout of the dispersion multiplexing spectrometer (DMS) is shown in Fig. 6. The optical components from input to output are the coded aperture (CA), the first set of relay lenses (L1), the multiplex hologram (MH), the second set of relay lenses (L2), and the CCD. The coded aperture is based on a Hadamard matrix of order $p = 12$ as shown in Fig. 2. An individual element within this mask is a square, sized 78×78 μm. The aperture is implemented as a pattern in chrome on a glass substrate, manufactured by Applied Image Group. The two sets of relay lenses form a 4-f system. Each set is composed of a pair of off-the-shelf 9 mm diameter lenses (Edmund Optics NT45-091 and NT45-092) in a Petzval configuration computationally optimized for low distortion with ZEMAX optical design software.

The multiplex hologram is a custom-designed three-grating diffractive element as described in Section 3. The three spectral bands defined by the gratings are specified in Table 1. The holograms are recorded using the angular multiplexing method.[17] The model that is used to design the holograms is based on Kogelnik's method.[18] We record the three holograms at wavelength λ_{rec} with proper incident angles for the recording beams θ_{ri}, for $i = 1, 2$, or 3. All the parameters are calculated inside the material with refractive index n, if it is not otherwise mentioned. We find the diffraction efficiency for one of the holographic gratings, and the result can be extended to all three multiplexed holograms.

Table 1. Spectral Band Data

	Center Wavelength (nm)	Spectral Bandwidth (1/e Full Width) (nm)	Peak Diffraction Efficiency (%)	Grating Period (lines/mm)
Red band	634	330	10.2	1150
Green band	531	222	9.27	1400
Blue band	452	155	14.6	1670

We use two beams with equal incident angles of θ_{r1} to record the hologram. This produces a grating vector, K_{g1}, with magnitude described by

$$K_{g1} = \frac{4\pi \sin(\theta_{r1})}{\lambda_{rec}}. \tag{6}$$

The hologram is then read with a collimated beam at wavelength λ with an incident angle of θ. We assume the reading beam has an arbitrary polarization. We, therefore, must calculate the response for both the TE (electric field perpendicular to the plane of incidence) and the TM (magnetic field perpendicular to the plane of incidence) polarizations. Kogelnik's method calculates the exact solution for the first-order diffraction from a volume grating.[18] This method is valid for the holograms recorded in samples of a few micrometers thickness, such as this case. The diffraction efficiency, η, from each hologram is

$$\eta = \gamma^2 \frac{\sin^2\left(\sqrt{\xi^2 + \gamma^2}\right)}{\xi^2 + \gamma^2}, \tag{7}$$

where γ and ξ are defined as

$$\gamma = \frac{\pi n_1 L_Z}{\lambda \cos(\theta)} \mathrm{PF}, \tag{8}$$

$$\xi = -\frac{(\lambda_B - \lambda) K_{g1}{}^2 L_Z}{8\pi n \cos(\theta)}. \tag{9}$$

In these equations PF, λ_B, L_Z, and n_1 are polarization factor, Bragg wavelength, hologram thickness, and refractive index modulation of the hologram, respectively. The polarization factor is defined as

$$\mathrm{PF} = \begin{cases} 1 & \text{for TE polarization} \\ \cos\left[2 \arcsin\left(\dfrac{\lambda \sin(\theta_{r1})}{\lambda_{rec}}\right)\right] & \text{for TM polarization} \end{cases}. \tag{10}$$

The Bragg wavelength, λ_B, is defined as the wavelength that is perfectly Bragg matched to the hologram with the incident angle θ, therefore

$$\lambda_B = \frac{\lambda_{rec} \sin(\theta)}{\sin(\theta_{r1})}. \tag{11}$$

The measured diffraction efficiency (η_{r1}) at the recording wavelength (λ_{rec}) and at the Bragg angle (θ_{r1}) is used to find n_1 from

$$n_1 = \frac{\arcsin\left(\sqrt{\eta_{r1}}\right)\lambda_{rec} \cos(\theta_{r1})}{\pi L_Z}, \tag{12}$$

where we assumed the measurement was performed using a beam with TE polarization.

To complete the model, we consider the effect of the polarization of the input beam. We assume we have equal power in TE and TM polarizations. Let us call the diffraction efficiency calculated for TE polarization η_{TE} and for TM polarization η_{TM}. Also, the total transmission from the interfaces between the air to the material and the material to air are considered as T_{TE} for TE polarization and T_{TM} TM polarization. Therefore the total diffraction efficiency (η_{Tot}) is

$$\eta_{Tot} = \frac{\eta_{TE} T_{TE} + \eta_{TM} T_{TM}}{\pi L_Z}, \tag{13}$$

where T_{TE} and T_{TM} can be found from

$$T_{TE} = 1 - \frac{\sin^2(\theta - \theta')}{\sin^2(\theta + \theta')}, \tag{14}$$

$$T_{TM} = 1 - \frac{\tan^2(\theta - \theta')}{\tan^2(\theta + \theta')}, \tag{15}$$

with θ' referring to the angle measured in the air.

For this derivation, we assumed that each hologram diffracts the input beam independently of the other holograms. This is a valid assumption when the diffraction efficiency of each hologram is not high (for example, less than 25%). When the diffraction efficiency of each hologram is high, all the diffraction components should be considered simultaneously using numerical methods such as rigorous coupled-wave analysis.

For the miniature spectrometer, the three holograms are recorded at $\lambda_{rec} = 532$ nm wavelength (measured in the air) in VRP-M holographic material from Integraf with an emulsion thickness of 6–7 μm. The holograms are designed to be used with an incident angle, θ, of 22.86°. This results in the total angles between the recording beams of 52.78°, 43.73°, and 35.66°. These correspond to Bragg wavelengths of 465, 555, and 675 nm, respectively. (Again, all wavelengths are measured in air.) Since the γ in Eq. (7) is a function of wavelength, the maximum diffraction efficiency is obtained at 452, 531, and 632 nm (for TE polarization) as listed in Table 1. The bandwidth three spectral bands defined by the gratings are also specified in Table 1.

Our detector is a color CCD (Unibrain Fire-i Board Camera with a Sony ICX-098BQ detector) with 5.6 μm pixels and a 640 × 480 resolution. The CCD is typical of the inexpensive detectors used in consumer grade devices like webcams, with standard Bayer color filters on the pixels, a maximum exposure time of 32 ms, and an 8-bit dynamic range. The optical components are assembled with a rigid polymer structure printed on a rapid prototyping system. Figure 7 shows a photograph of the assembled system.

The data recorded by the DMS must be processed in two steps to form a spectral estimation of the input source. The first step forms a spectral estimate for each of the three spectral bands. The second step combines the three estimates into a single spectral

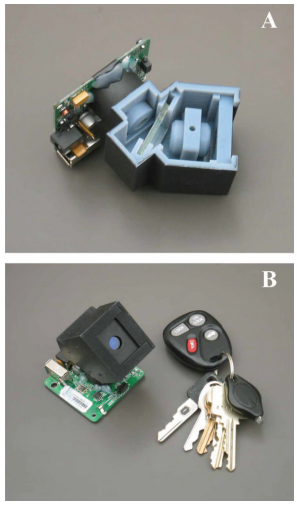

Fig. 7. (Color online) A: Photograph of the dispersion multiplexing spectrometer's internal structure. B: Photograph of the spectrometer with keys to show approximate size.

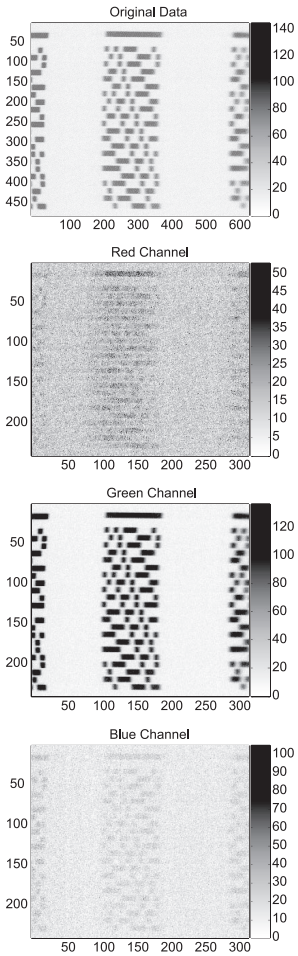

Fig. 8. Original 550 nm data captured by CCD (top) and unprocessed data separated into the RGB color channels (lower images).

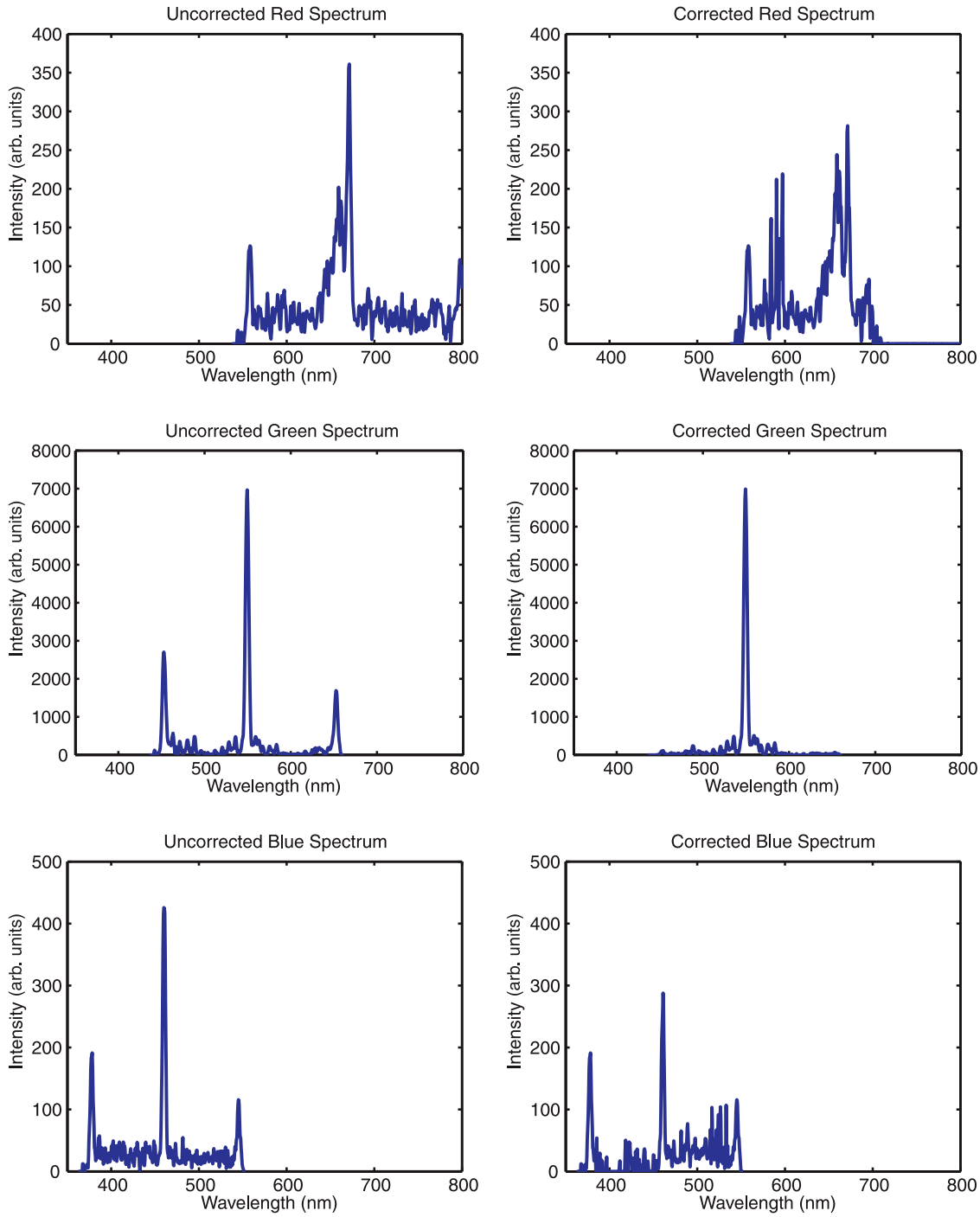

Fig. 9. (Color online) Spectra for 550 nm input, RGB color channels separated by rows. Results from coded aperture inversion appear in the left column, and the results after applying the dispersion multiplexing correction appear in the right column. Note the differing scale of the y axis for the different color channels.

estimate. For the first step, we assume that the camera records three separate images of the aperture-coded spectrum in RGB. We perform the data inversion procedure described in Section 2 of the paper to calculate the spectrum corresponding to each of these images. We then apply the dispersion multiplexing correction algorithm described in Section 3 to these three spectra. Care is taken to preserve the spatial relation between reconstructed spectral bands so that the kth sample in one spectral band corresponds to the kth sample in another, which are both related to a specific column on the detector. To determine the relationship between the columns of the detector and wavelength, we record a set of data by sweeping a monochromator input to the spectrometer over the visible wavelength range. This gives us the $(\lambda_r, \lambda_g, \lambda_b)$ values to evaluate the filter functions in Eq. (5). Solving the system of equations in Eq. (5)

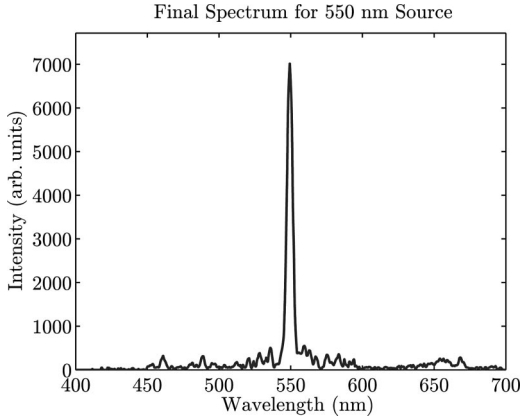

Fig. 10. Fully processed spectrum measured from a 550 nm source.

yields the corrected RGB spectra, which are then combined to form the complete spectral estimate.

The spectral resolution of the DMS is different for the three spectral bands. The system model developed in the ZEMAX software package provides values for the linear dispersion of the three gratings at the detector plane. For the DMS prototype, the limiting factor for the spectral resolution is the 78 μm size of the mask elements of the coded aperture, rather than the optical spot size or the pixel size on the detector. With the linear dispersion values and the feature size of the aperture mask, it is possible to calculate the resolutions of the three spectral bands. Resolution ($\Delta\lambda$) for a single band is calculated with Eq. (16)—the product of the linear dispersion of the grating at the detector ($d\lambda/dx$) with the feature size of the mask (δ).

$$\Delta\lambda = \frac{d\lambda}{dx}\,\delta. \tag{16}$$

Values for linear dispersion of the RGB bands from our ZEMAX model are 43.3, 36.3, and 30.7 nm/mm. With a 78 μm feature size, the RGB resolutions are 3.37, 2.83, and 2.39 nm. A reduction in the feature size, combined with a increase in mask complexity (basing it on a higher-order Hadamard matrix) would increase both spectral resolution and light throughput of the instrument.

5. Experimental Data

To demonstrate the data processing procedure, a monochromatic source of wavelength 550 nm and FWHM width of 4.5 nm was measured with the DMS system. The light source was a monochromator with spectral bandwidth verified by an Ocean Optics USB 2000 spectrometer. Figure 8 shows the original data recorded by the CCD as well as the three images formed by separating the RGB pixels into individual images. The patched look of the original image is due to the response of the Bayer pattern filters on the CCD pixels. The green channel image in Fig. 8 clearly shows the response of all three grating periods to the monochromatic input. The Hadamard-type pattern in the center is the response of the green grating, while the partial pattern at the right is due to the blue grating, and the partial pattern at the left is the red grating—each near the edge of their respective spectral ranges. The Hadamard patterns are visible in all the color channel images because 550 nm falls within the combined spectral response of their respective Bayer filters and grating diffraction efficiencies. Figure 9 shows the result of the coded aperture inversion procedure applied to the RGB images in the left column and the spectra after correcting for the dispersion multiplexing overlap on the right column. The scale of the y axes is adjusted to show the aliasing caused by Bayer filter responses. The green channel in the right column shows the response to the 550 nm input, while the red and blue channels in the right column show the noise floor of the system. Figure 10 shows the spectral estimate of the 550 nm input, a combination of the three spectra in the right column of Fig. 9. Analysis of the data plotted in Fig. 10 shows a full width of 4.7 nm at half of the maximum intensity value.

A fluorescent ceiling lamp was used as a demonstration spectral source with features across the

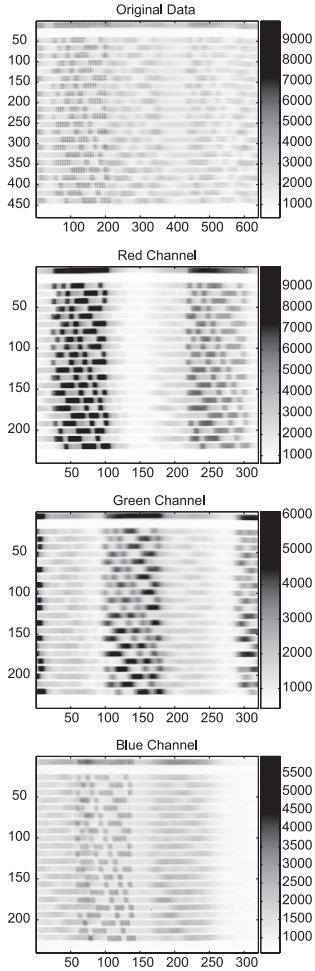

Fig. 11. Original fluorescent light data captured by a CCD (top) and unprocessed data separated into the RGB color channels (lower images).

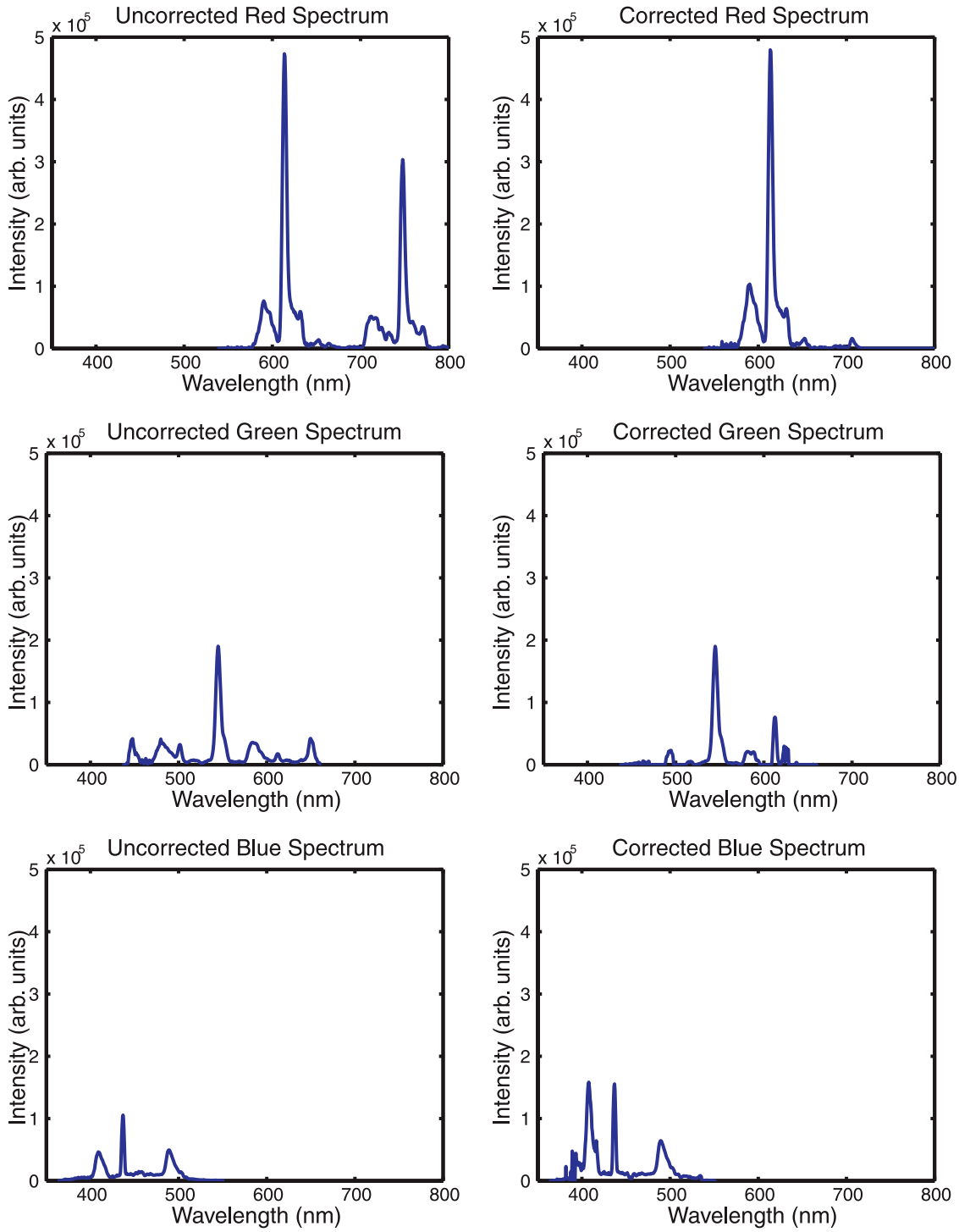

Fig. 12. (Color online) DMS spectra for a fluorescent lamp. Results from coded aperture inversion (left column) and dispersion multiplexing correction (right column). The rows show the separate RGB color channels.

entire spectral range of the DMS. The original image as well as the separated RGB color channel images appear in Fig. 11. The separated RGB channel images show the system response to spectral features within the different spectral regions. Figure 12 shows the Hadamard-reconstructed spectra in the left column and the spectra corrected for dispersion multiplexing in the right column. Again, the spectra for the individual RGB color channels are separated across the rows of Fig. 12. The fully processed fluorescent light spectrum appears in Fig. 13, above a spectrum of the same lamp measured with an Ocean Optics USB 2000 spectrometer. Both instruments have varying spectral intensity responses due to the characteristics of the individual diffractive elements and detectors used. Neither of the spectra in Fig. 13 are

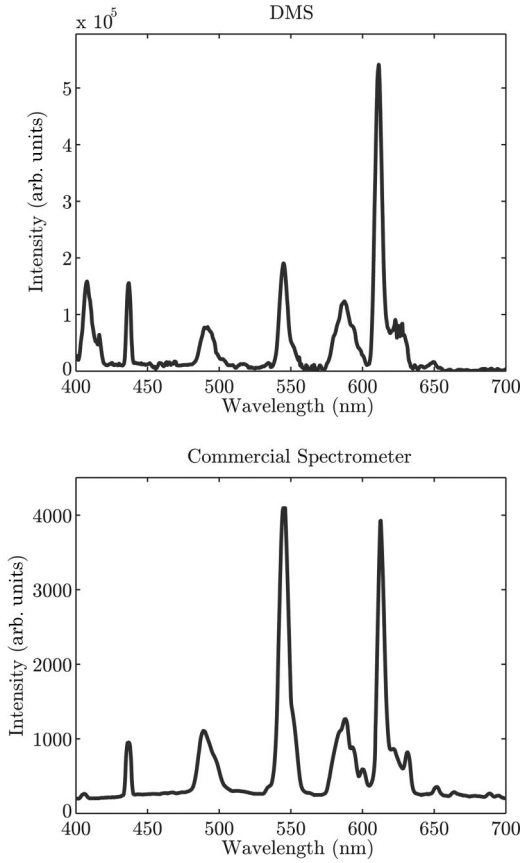

Fig. 13. Fully processed spectrum of a fluorescent lamp from the DMS (top) compared with a measurement made with a commercial spectrometer (bottom).

intensity corrected, so the relative heights of the peaks in the spectra are different.

6. Summary

We have presented a spectrometer design, which implements two different multiplexing techniques, allowing us to miniaturize the system versus a traditional spectrometer design. One multiplexing technique is implemented in the aperture, utilizing an aperture mask to provide high light throughput without sacrificing spectral resolution. This allows us to collect a sufficient signal with small diameter optics and a small detector. The other multiplexing technique is implemented in the dispersive element, utilizing a hologram with three grating periods recorded in it. With dispersion multiplexing, we measure three different spectral bands simultaneously, each dispersed across the full extent of the detector. This allows us to increase the total spectral range measured with a small detector. Both of these techniques can be used independently in spectrometer design, though they do compliment each other in our design.

This work was performed with the support of grant N01-AA-23013 from the National Institute of Alcoholism and Alcohol Abuse and grant W911NF-04-1-0319 from DARPA-MTO and ARL-SEDD.

References

1. H. Owen, D. E. Battey, M. J. Pelletier, and J. B. Slater, "New spectroscopic instrument based on volume holographic optical elements," in Proc. SPIE **2406,** 260–267 (1995).
2. D. J. Brady, "Multiplex sensors and the constant radiance theorem," Opt. Lett. **27,** 16–18 (2002).
3. S. D. Schwab and R. L. McCreery, "Versatile, efficient Raman sampling with fiber optics," Anal. Chem. **56,** 2199–2204 (1984).
4. J. Zhao, "Image curvature correction and cosmic removal for high-throughput dispersive Raman spectroscopy," Appl. Spectrosc. **57,** 1368–1375 (2003).
5. M. J. E. Golay, "Multi-slit spectrometry," J. Opt. Soc. Am. **39,** 437–444 (1949).
6. A. Girard, "Spectrometre a grilles," Appl. Opt. **2,** 79–87 (1963).
7. R. N. Ibbett, D. Aspinall, and J. F. Grainger, "Real-time multiplexing of dispersed spectra in any wavelength region," Appl. Opt. **7,** 1089–1094 (1968).
8. M. O. Harwitt and N. J. A. Sloane, *Hadamard Transform Optics* (Academic, 1979).
9. A. Wuttig and R. Riesenberg, "Sensitive Hadamard transform imaging spectrometer with a simple MEMS," in Proc. SPIE **4881,** 167–178 (2002).
10. Q. S. Hanley, P. J. Verveer, and T. M. Jovin, "Spectral imaging in a programmable array microscope by Hadamard transform fluorescence spectroscopy," Appl. Spectrosc. **53,** 1–10 (1999).
11. M. E. Gehm, S. T. McCain, N. P. Pitsiantis, D. J. Brady, P. Potuluri, and M. E. Sullivan, "Static 2D aperture coding for multimodal multiplex spectroscopy," Appl. Opt. **54,** 2965–2974 (2006).
12. A. S. Hedayat, N. J. A. Sloane, and J. Stufken, *Orthogonal Arrays: Theory and Applications* (Springer-Verlag, 1999).
13. D. J. Schroeder, *Astronomical Optics* (Academic, 1987).
14. S. T. McCain, M. E. Gehm, Y. Wang, N. P. Pitsianis, and D. J. Brady, "Coded aperture Raman spectroscopy for quantitative measurements of ethanol in a tissue phantom," Appl. Spectrosc. **60,** 663–671 (2006).
15. *HoloPlex Holographic Transmission Grating,* Technical Rep. 1201 (Kaiser Optical Systems, Inc., 2001).
16. B. E. Bayer, "Color imaging array," U.S. patent 3,971,065 (20 July 1976).
17. G. Barbastathis and D. Psaltis, *Volume Holographic Multiplexing Methods* (Springer, 2000), pp. 21–59.
18. H. Kogelnik, "Coupled wave theory for thick hologram grating," Bell Syst. Tech. J. **48,** 2909–2948 (1969).